Submitted to Nuclear Physics

LBL-2313
Preprint

DIFFERENTIAL $K_L \rightarrow K_S$ REGENERATION CROSS SECTION IN COHERENT PRODUCTION MODEL AND OPTICAL MODEL

W. L. Wang and Fumiyo Uchiyama

October 1973

Prepared for the U.S. Atomic Energy Commission
under Contract W-7405-ENG-48

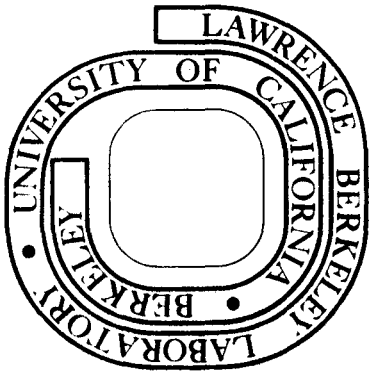

LBL-2313

DISCLAIMER

DIFFERENTIAL $K_L \longrightarrow K_S$ REGENERATION CROSS SECTION IN COHERENT PRODUCTION MODEL AND OPTICAL MODEL*

W. L. Wang and Fumiyo Uchiyama

Lawrence Berkeley Laboratory
University of California
Berkeley, California 94720

October 1973

Abstract

We investigate the high-energy $K_L \rightarrow K_S$ regeneration process in nuclei in terms of a coherent production model. The angular distribution of the regenerated K_S is calculated for Pb and Cu at an incident momentum of 4 GeV/c. The experimental data are well reproduced. We have also performed an optical-model calculation which explicitly treats K_L as a mixture of K_o and $\bar{K}_o$ particles. We show that it is not necessary to introduce a large neutron skin in the above nuclei to interpret the data, if the finite range of strong interaction is taken into account properly in the density distribution. The coherent production model and the optical model, with seemingly very different physical interpretations, give very similar results. We also show that these models represent two ways of summing the multiple scattering series in the particular case of $K_L \rightarrow K_S$ regeneration. In conclusion, we discuss the unique and important feature of using nuclear regeneration scattering to study scattering theories, as compared to other high-energy particle-nucleus scattering.

*Work performed under the auspices of the U. S. Atomic Energy Commission.

1. Introduction

It is interesting to note that the regeneration phenomenon of the long-lived kaon K_L particle in a nuclear medium has been of interest even before the discovery of the K_L particle itself[1]). The phenomenon is predicted in the particle-mixture theory of Gell-Mann and Pais[2]), in which a neutral kaon K_o, or its antiparticle $\bar{K}_o$, produced in strong interaction is an equal mixture of K_L and K_S (the short-lived component of a neutral kaon). The half-life for K_L is about 5×10^{-8} sec and that for K_S is about 10^{-10} sec. Therefore, when a K_o beam is allowed to decay for a duration of several K_S half-lives, we obtain a beam of nearly pure K_L particles with half the intensity. If these remaining K_L particles are scattered through a nuclear medium, the unequal scattering amplitudes of K_o and $\bar{K}_o$ will regenerate K_S particles. This "bizarre manifestation of the mixing of K_o and $\bar{K}_o$"[3]) was finally verified in the first transmission regeneration measurement by Good et al.[4]), who described the particle-mixture theory as "one of the most astonishing and qratifying successes in the history of the elementary particles".

We now turn to some recent experimental data. The energy dependence of the forward $K_L \rightarrow K_S$ regeneration has been measured and analyzed for Cu by Böhm et al.[5]). The angular distributions of the regenerated K_S from Cu and Pb have been measured by Foeth et al.[6]), who also analyzed their data in terms of an optical model which was first used by Böhm et al.[5]). In this optical model analysis, it was concluded that an appreciable neutron excess in the nuclear surface is required to fit the data, and that the neutron regeneration power is five times as large as that of the proton[5]).

In this work, we shall analyze the differential cross section in a different approach. Aside from the optical model description, it seems to be also natural to discuss the regeneration process as particle coherent production, in which the K_S is coherently produced by a high energy K_L particle. For this purpose, we use the coherent production model as introduced by Kölbig and Margolis[7]. We shall describe both the coherent production model and the optical model and present our results in Sec. 2. We study the optical-model calculation in more detail and show that there is no evidence for a large neutron skin, if a proper choice of proton distribution is used. The neutron regeneration power could also be much smaller. We also demonstrate briefly the equivalence between the two models, as applied to the $K_L \to K_S$ regeneration process. The concluding remarks are given in Sec. 3, where we point out some particular features in the regeneration scattering which may be of interest in the study of high energy particle-nucleus scattering.

2. Model calculations

In this section we present the formalism and the numerical results of both the coherent production model and the optical model. The two formalisms are then shown to be equivalent. We first discuss the coherent production model[7]) for the nuclear $K_L \to K_S$ regeneration.

2.1. COHERENT PRODUCTION MODEL

The coherent production model has been shown to reproduce the energy dependence of the forward regeneration cross sections[8]). The intuitive physical picture is given in fig. 1. The incident K_L particle is first scattered elastically by the nucleons and then changes itself into a K_S particle through some exchange mechanism between the K_L and the nucleons. The K_S is then scattered by the nucleons in its path out of the nucleus. Since the regeneration process is much weaker than the elastic scattering, the regeneration event probably does not happen more than once inside the nucleus (one-step approximation). If we further neglect nucleon-nucleon correlations, we may write the scattering amplitude as a coherent sum of the scattering amplitudes resulting from regeneration by each bound nucleon. The differential cross section for the coherent regeneration process may be written as[7])

$$\left(\frac{d\sigma}{dt}\right)_{K_L A \to K_S A} = \left(\frac{d\sigma_o}{dt}\right)_{t=0} \left|F(t)\right|^2 , \qquad (1)$$

where $t = -$ (momentum transfer)^2 and $(d\sigma_o/dt)_{t=0}$ is the forward regeneration cross section of a nucleon. The amplitude $F(t)$ is related to the multiple

scattering of the incident and outgoing particles with the nucleus, and also to the fact that the regenerating nucleon is bound. We may write F(t) as

$$F(t) = \int_0^\infty e^{i\vec{q}\cdot\vec{b}}\, T(\vec{b}) e^{-\frac{1}{2}(1-i\alpha_{KN})\,\sigma_{KN} T(\vec{b})}\, d^2\vec{b} \quad , \tag{2}$$

where $\vec{q}$ is the momentum transfer, $q^2 = -t$, and $\vec{b}$ the impact parameter. In eq. (2), the neutron and proton distributions are taken to be the same. The total K_L- and K_S-nucleon average cross sections are the same (neglecting weak interactions) and denoted as σ_{KN} ,

$$\sigma_{KN} = \left(\frac{Z}{A}\right) \sigma_{Kp} + \left(1 - \frac{Z}{A}\right) \sigma_{Kn} \quad , \tag{3}$$

where Z is the number of protons and A is the number of nucleons, and σ_{Kp} and σ_{Kn} are the K-proton and K-neutron total cross sections, respectively. In eq. (2), we denote the real to imaginary ratio of the K_L-nucleon forward scattering amplitude as α_{KN}, which may be related to various K-nucleon cross sections by use of strong exchange degeneracy hypothesis[9]) and the optical theorem, as described in ref. [8]). (Values of the parameters used in our calculations at 4 GeV/c are listed in Table 1.) The nuclear effects enter in the form of the two-dimensional density $T(\vec{b})$. We have defined

$$T(\vec{b}) = A \int_{-\infty}^{\infty} \rho(\vec{r})\, dz \tag{4}$$

where $\rho(\vec{r})$ is the nuclear density distribution (normalized to unity). The integration in eq. (4) is along the direction of incident momentum z. For the nuclei of interest here, we assume a spherical symmetric Woods-Saxon density distribution

$$\rho(r) = \rho_o \{1 + \exp[(r-c)/a]\}^{-1} \quad , \tag{5}$$

where ρ_o is the density normalization, c the half-radius, and a the diffuseness. Here we have assumed the same density distribution for both neutrons and protons. Although there might be a possibility of a larger neutron radius (about 0.3 fm larger for Pb and 0.1 fm larger for Cu)[10], this difference should not be important in our study of the main characteristics of the regeneration process.

It is important to note that the form of the nuclear density $\rho(r)$ in eq. (5) is determined from electron scattering[11]. It is identified with the charge distribution, and therefore the proton distribution, as seen by a point particle. It has been found, as in proton scateering, that, due to finite range of strong interaction, the effective nuclear density is different from that determined from electron scattering. The effects of the finite range interaction are given by[11]

$$c = c_{electron} + (0.8 \pm 0.3) \text{ fm} \quad , \tag{6}$$

and

$$a = 0.6 \sim 0.7 \text{ fm} \quad , \tag{7}$$

where $c_{electron}$ is the half-radius determined from electron scattering. Assuming that forward diffractive Kp and pp elastic scattering depends on the "size" of the particles, we find that kaons are roughly as large as protons. For Cu and Pb nuclei, we therefore choose $c = 1.2\ A^{1/3}$ fm and $a = 0.6$ fm, as consistent with eqs. (6) and (7). [This choice of effective nuclear density has been shown to reproduce the forward regeneration cross section in the energy range 2.5 - 7.5 GeV/c (ref. [8]).]

We now present our results for the coherent production model as described above. The parameters we need are in Table 1. The averaged forward regeneration cross section on a nucleon $(d\sigma_o/dt)$ may be expressed as

$$\left(\frac{d\sigma_o}{dt}\right)_{t=0} = \frac{\pi}{k^2} \left| \left(\frac{Z}{A}\right) f_{K_L p \to K_S p}(o) + \left(1 - \frac{Z}{A}\right) f_{K_L n \to K_S n}(o) \right|^2 , \qquad (8)$$

where k is the K_L-momentum in the c.m. system, and $f_{K_L p \to K_S p}(o)$ and $f_{K_L n \to K_S n}(o)$ are the forward regeneration amplitudes of a proton and a neutron, respectively. The proton amplitude has been determined by Brody et al.[12]), and by Darriulat et al.[12]). If we assume that the neutron amplitude is given by

$$f_{K_L n \to K_S n} = \gamma f_{K_L p \to K_S p} , \qquad (9)$$

where γ is a real constant, we then have

$$\left(\frac{d\sigma_o}{dt}\right)_{t=0} = \left(\frac{Z}{A}\right)^2 \left[1 + \gamma \left(\frac{A}{Z} - 1\right)\right]^2 \left(\frac{d\sigma_H}{dt}\right)_{t=0} , \qquad (10)$$

where $(d\sigma_H/dt)_{t=0}$ is the proton regeneration cross section given in Table 1. We shall call the proportionality constant γ as the neutron enhancement factor. This factor is taken to be 1 in ref. [8]), and is found to be larger than 2 in ref. [6]).

In our calculations, we choose $\gamma = 1.26$ and 1.5 for Cu and Pb respectively, in order to reproduce the magnitude of the differential cross section. It is important to point out that the value for γ being greater than

unity should not be taken as definite evidence for a much larger regeneration power of the neutron, as compared to that of the proton; it relies directly on the value of $(d\sigma_H/dt)_{t=0}$ used. The value we quote in Table 1 for $(d\sigma_H/dt)_{t=0}$ is a median value of several measurements with very large uncertainty (as large as ±50%)[12]. In our calculation, the value of γ can vary from 1.0 to about 2.0, depending on the value of $(d\sigma_H/dt)_{t=0}$ we choose within experimental accuracy.

The differential cross sections for Cu and Pb are shown as the solid lines in fig. 2. It is interesting to note that both the magnitude and the diffraction pattern are well reproduced. Here we have used the term "diffraction" only to indicate a differential cross section that is strongly forward-peaked. The position of the diffraction minima depends on the nuclear radius. The value of $\alpha_{KN} = -0.11$ from ref. [8]) is used. A larger value of $\alpha_{KN} = -0.22$ is shown to fill up the minimum (see the dashed lines in fig. 1). The dash-dot lines are the results of the optical-model calculation to be discussed later.

In this calculation, we have chosen γ [see eq. (9)] to be greater than 1 in order to reproduce the magnitude of the differential cross section, but it predicts a larger forward regeneration cross section than that obtained from the transmission measurements (as represented by the squares in fig. 1). The choice of $\gamma = 1$, which reproduces the forward regeneration cross section would give a smaller differential cross section for all angles. The discrepancy at the forward angle remains unresolved. It would, however, be rather unexpected if the cross section should bend over (as the case in Cu) near very small momentum transfer.†

†It is interesting, however, to observe that, if the turning-over at small q^2 is real, i.e. not due to statistical errors, it may suggest a helicity-flip contribution in the nuclear regeneration process. There is some evidence for a helicity-flip contribution in proton regeneration experiments[13]). The helicity-flip effects might be more readily seen, due to better statistics and possible coherent enhancement in nuclear regeneration.

In this section we have shown that the coherent production model is quite adequate to describe the angular distribution of $K_L \rightarrow K_S$ regeneration. This diffraction pattern depends mainly on the nuclear size, particularly within the first minimum. The parameters from the K-nucleon elastic scattering, i.e. α_{KN} and σ_{KN}, also affect the magnitude of the second maximum, although only rather weakly. We would like to emphasize that the coherent production model provides us a convenient framework to study separately the basic nucleon regeneration process and the nuclear effects, since these two factors are separated in the formalism and we have shown that their effects on the differential cross section are also independent.

In order to compare our results with those obtained in ref. 6, we would first like to describe the optical model formalism.

2.2. OPTICAL MODEL

The optical model description follows closely the particle-mixture theory. In the nucleus, the strong interaction immediately selects out states with definite strangeness and, therefore, it is more convenient to write the K_L and K_S state as linear combinations of K_o and $\bar{K}_o$ states:

$$|K_L\rangle = \frac{1}{\sqrt{2}} [|K_o\rangle - |\bar{K}_o\rangle] \quad , \tag{11}$$

and

$$|K_S\rangle = \frac{1}{\sqrt{2}} [|K_o\rangle + |\bar{K}_o\rangle] \quad . \tag{12}$$

It is known that K_o and $\bar{K}_o$ interact differently with nucleons, which gives rise to the nucleon regeneration phenomenon. Similarly, if a K_L particle is scattered by a nucleus, each component, K_o and $\bar{K}_o$, may also have different scattering

amplitudes, F and $\bar{F}$, respectively. This difference in the amplitudes gives rise to the nuclear diffraction regeneration phenomenon[4]. We may write the scattered wave from K_L-nucleus scattering as

$$|\psi_{SC}\rangle = \frac{1}{\sqrt{2}} [F|K_o\rangle - \bar{F}|\bar{K}_o\rangle] \quad , \tag{13}$$

or, in terms of $|K_L\rangle$ and $|K_S\rangle$ again, as

$$|\psi_{SC}\rangle = \frac{1}{2} [(F+\bar{F})|K_L\rangle + (F-\bar{F})|K_S\rangle] \quad . \tag{14}$$

From this equation, we find the regeneration amplitude for K_S as

$$F_R^{Opt} = \frac{i}{2} [F-\bar{F}] \quad . \tag{15}$$

We describe this process in fig. 3, where K_o and $\bar{K}_o$, due to opposite strangeness, are scattered independently by the nucleus with scattering amplitudes F and $\bar{F}$, respectively. The optical potentials may be related to K_o- and $\bar{K}_o$-nucleon interactions. At high energies it is appropriate to use a semiclassical description[14]. We may write the scattering amplitudes as

$$F(q^2) = \frac{ik}{2\pi} \int e^{i\vec{q}\cdot\vec{b}} [1 - e^{iP(\vec{b})}] \, d^2b \tag{16}$$

where $P(\vec{b})$ is a phase shift function. In the case of K_o-nucleus scattering, we may write

$$P(\vec{b}) = \frac{i}{2}\left[\frac{Z}{A} (1-i\alpha_{K_op}) \, \sigma_{K_op} T_p(\vec{b}) + (1 - \frac{Z}{A}) \, (1-i\alpha_{K_on})\sigma_{K_on} T_n(\vec{b})\right] \tag{17}$$

where σ_{K_oN} are the total K_o-N cross sections, α_{K_oN} are the ratios of the real

to imaginary parts of the forward K_o-N scattering amplitudes. The two-dimensional densities $T_N(\vec{b})$ are related by eq. (4) to the proton and neutron densities, which are assumed to have a Woods-Saxon form. This specifies our K_o-nucleus scattering amplitudes. For $\bar{K}_o$-nucleus scattering, we also use eq. (16), with the K-nucleon parameters in $P(\vec{b})$ appropriately changed for $\bar{K}_o$. We may now calculate the regeneration amplitude F_R^{opt} by eq. (15). In order to compare with the results in ref. 6 we use their parameters at 4 GeV/c (as listed in Table 1) except that we assume the neutron density to be the same as the proton density (with different normalizations). We use $c = 1.2\ A^{1/3}$ fm and $a = 0.6$ fm, the same as those in the coherent production model calculation. The regeneration cross section is defined as

$$\left(\frac{d\sigma}{dt}\right)_{K_L A \to K_S A} = \left(\frac{\pi}{4k^2}\right) \left|F(q^2) - \bar{F}(q^2)\right|^2 \quad . \tag{18}$$

The results of our optical-model calculation are shown as the dash-dot lines in fig. 2. These results are essentially the same as those in ref. 6, where different proton and neutron radii are used. It is clear that the necessity of a larger neutron radius in ref. 6 is only due to their parametrization of the proton density distribution, which is obtained directly from electron scattering without modification [see eqs. (6) and (7)].

We would like to point out that the parameters used in the optical model calculation are consistent with our choice of the paramter α in the coherent production model. The relations between the parameters in the two models

are given in Table 1. The neutron regeneration enhancement factor γ is about 2.2 in the optical model calculation. We recall that this value is larger than what we have in the coherent production model. However, it is clear, from fig. 2, that a smaller value of γ would give a better fit to the data since it reduces the magnitude of the cross section without changing the main diffraction pattern (similar to the role it plays in the coherent production model).

We now have shown that the optical model also provides an adequate description of the nuclear regeneration process, including the diffraction pattern which is quite sensitive to the scattering amplitudes for K_o and $\bar{K}_o$.

Before presenting a more detailed study of the two models, we would like to point out a simple scaling property in the diffraction patterns shown in fig. 4. First we observe that the forward scattering cross sections of Pb and Cu satisfy approximately the relation

$$\frac{\left(d\sigma_{A_1}/dt\right)_{t=0}}{\left(d\sigma_{A_2}/dt\right)_{t=0}} = \left(\frac{c_1}{c_2}\right)^4 , \qquad (19)$$

where c_i are the half-radii of the target nuclei A_i. This relation, eq. (19), should hold true in elastic scattering from a strongly absorptive sphere of radius c. It is interesting that the diffraction regeneration should also obey this rule. Another property of strong absorption is that the momentum transfer at the diffraction minimum q_{min} is inversely proportional to the radius, i.e. $q_{min} R \approx \text{constant}$[15].

The results of the above observation are shown in fig. 4, which demonstrates the scaling property very clearly within the first minimum. As we have pointed out, the diffraction pattern (at small momentum transfer) sets a very restrictive range for the nuclear radius. In the coherent production model, this feature allows us to discuss separately the effects of the neutron regeneration enhancement factor γ: We determine R from the diffraction pattern and γ from the magnitude of the cross section. This simple separation is, however, not provided by the optical model. As we shall see later, the diffraction-like pattern shown in fig. 4 actually has a much more complex feature than is usually expected in a simple diffractive elastic scattering.

In the following, we show the properties in the optical-model amplitudes which lead to the diffraction-like pattern in the regeneration cross section. There is no a priori reason for the regeneration process to be diffraction-like, since the difference of two diffractive amplitudes may not be diffractive. We may relate the two optical-model amplitudes as

$$\bar{F}(q^2) = e^{i\Phi(q^2)} \left|\frac{\bar{F}(q^2)}{F(q^2)}\right| F(q^2) \quad , \tag{20}$$

and then the regeneration cross section in eq. (18) may be written as

$$\left(\frac{d\sigma}{dt}\right)_{K_L A \to K_S A} = \frac{1}{4}\left(\frac{d\sigma_A}{dt}\right)_{K_o}\left[1 - 2\cos\Phi(q^2)\left|\frac{\bar{F}(q^2)}{F(q^2)}\right| + \left|\frac{\bar{F}(q^2)}{F(q^2)}\right|^2\right] \quad , \tag{21}$$

where we have defined the elastic scattering cross section of K_o on the target nucleus as

$$\left(\frac{d\sigma_A}{dt}\right)_{K_o} = \frac{\pi}{k^2}\left|F(q^2)\right|^2 \quad . \tag{22}$$

Since K-nucleus scattering at high energy is mainly diffractive, we expect the regeneration cross section to be also diffractive only if $\Phi(q^2)$ and $|\bar{F}(q^2)/F(q^2)|$ are independent of q^2. We show these quantities in fig. 5, where the q^2-dependence is small only in low q^2 region. We, thus, do not have a diffraction pattern for the regeneration process. We would further note that the cancellations in eq. (21) are very important since the regeneration cross section is small compared to the elastic scattering cross section, e.g., for Pb

$$\left(\frac{d\sigma}{dt}\right)_{K_L A \to K_S A} \approx 0.01 \left(\frac{d\sigma_A}{dt}\right)_{K_o} . \tag{23}$$

The fact that eq. (21) provides us with a relation between $(d\sigma/dt)_{K_L A \to L_S A}$ and the elastic cross sections $(d\sigma_A/dt)_{K_o}$ of $(d\sigma_A/dt)_{\bar{K}_o}$ is useful since we may also calculate $(d\sigma_A/dt)_{K_L A \to K_S A}$ in the coherent production model, which is not directly related to the optical-model quantities on the right-hand side of eq. (21). This is a unique feature of regeneration scattering.

It is interesting to note that the results obtained from the two models discussed are practically identical. This may seem somewhat surprising because of their apparent assumption of different regeneration mechanisms, one with a one-step production mechanism and the other with a gradual change in the scattering wave along the path of interaction. In the next section, we shall show that in fact these two formalisms are formally equivalent, the difference being the approximations which give the final closed forms for the scattering cross sections, as given by eqs. (1) and (18).

2.3. EQUIVALENCE OF THE TWO FORMALISMS

The basic two-body scattering amplitude for $K_L \to K_S$ regeneration is shown in fig. 6. The regeneration amplitude is shown to be related to the difference between the K_o- and $\bar{K}_o$-nucleon elastic scattering amplitudes. If we now sum over the nucleons in the nucleus on both sides of fig. 6, we obtain the results in fig. 7, where the left-hand is formally identical to the amplitude obtained in the coherent production process and the right-hand side is just the optical-model amplitude. It is, therefore, clear that the two formalisms are equivalent. From these observations, the difference between the two models is only due to the approximations in reducing both sides of fig. 7 to eq. (2), and eqs. (15) and (16), respectively.

It is further interesting to note that the high energy semiclassical approximations (such as short-range interaction, optical limit, impulse approximation and forward scattering assumption, etc.) inherent in both models are quite similar. One obvious extra assumption in the coherent production model, as in eq. (1), is the one-step regeneration approximation; this should be valid since the regeneration process is very weak and the next multi-step correction involves three-step ($K_L \to K_S \to K_L \to K_S$) processes. The fundamental difference between the models, however, remains clear: The coherent production model aims its attention directly on the small regeneration amplitude, and the optical model described the complete scattering phenomenon which then gives rise to a small regeneration amplitude. The optical model, therefore, serves as a more

rigorous test to various nuclear multiple scattering theories, especially at lower energies and lower-mass nuclei, where more detailed formulation of the scattering theory becomes necessary. Nevertheless, the coherent production model may be more accurate in a specific nuclear scattering theory, simply due to less sensitivity to delicate cancellations.

As a final comparison between the two models, let us study their scattering amplitudes in more detail. For this purpose we would re-express the various K-nucleon parameters in the coherent production model in terms of the optical-model parameters $P(b)$ and $\bar{P}(b)$. By definition, we write the average forward nucleon regeneration amplitude $f_{K_L N \to K_S N}(o)$ as, from eqs. (1) and (8).

$$f_{K_L N \to K_S N}(o)\ T(\vec{b}) = \left(\frac{Z}{A}\right) f_{K_L p \to K_S p}\ T_p(\vec{b}) + \left(1 - \frac{Z}{A}\right) f_{K_L n \to K_S n}\ T_n(\vec{b}) \tag{24}$$

where we have restored the dependence on separate proton and neutron distributions, which are assumed to be equal (within a normalization) in eq. (1). We also use the following definition of the nucleon regeneration amplitude:

$$f_{K_L N \to K_S N}(o) = \frac{i}{2}\left[f_{K_o N}(o) - f_{\bar{K}_o N}(o)\right] \quad , \tag{25}$$

where $f_{K_o N}(o)$ and $f_{\bar{K}_o N}(o)$ are K_o- and $\bar{K}_o$-nucleon forward scattering amplitudes, which are then related to the corresponding total cross sections. By algebraic manipulations, we may write the coherent regeneration amplitude $F_R^{coh}(q^2)$ as,

$$F_R^{coh}(q^2) = \frac{ik}{2\pi}\int d^2 b\ e^{i\vec{q}\cdot\vec{b}}\ \frac{1}{2}\left\{\left[P(\vec{b}) - \bar{P}(\vec{b})\right] \exp\frac{i}{2}\left[P(\vec{b}) + \bar{P}(\vec{b})\right]\right\} \tag{26}$$

where $P(b)$ and $\bar{P}(b)$ are defined in eq. (13). In the optical model, we have

$$F_R^{opt}(q^2) = i\left(\frac{ik}{2\pi}\right) \int d^2 b\, e^{i\vec{q}\cdot\vec{b}} \left[\frac{e^{i\bar{P}(\vec{b})} - e^{iP(\vec{b})}}{2}\right] \quad . \tag{27}$$

Equations (26) and (27) now allow us to study in detail both models for the of a unique set of optical-model parameters.

In the following example, we show the difference in these models for the case of Pb. In fig. 8, we plot the integrands from eqs. (26) and (27) as defined as, (assuming spherically symmetric densities),

$$I_2^{coh}(b) = \frac{i}{2} \left[P(b) - \bar{P}(b)\right] e^{\frac{i}{2}\left[P(b) + \bar{P}(b)\right]} \quad , \tag{28}$$

and

$$I^{opt}(b) = \frac{1}{2} \left[e^{iP(b)} - e^{i\bar{P}(b)}\right] \quad . \tag{29}$$

It is clear that $I_2^{coh}(b)$ and $I^{opt}(b)$ are equal in the limit that both $P(b)$ and $\bar{P}(b)$ are very small or equal. We find that, for small $b \lesssim R$, both $P(b)$ and $\bar{P}(b)$ are large and not equal.† In fig. 8, it is rather unexpected to see that the two models, using the same parameters, are almost indistinguishable. It is important to note that the parametrizarion of the coherent production model in terms of P and $\bar{P}$ [eq. (28)] is not the same as that given by eq. (1). In the coherent production model, we always use linear combinations of P and $\bar{P}(b)$ as the parameters, but not separately. According to eqs. (1) and (2), we may define an equivalent integrand, as $I_2^{coh}(b)$ and $I^{opt}(b)$, directly for the coherent production model: We have

†For example, $\bar{P}(b=0) = 0.0 + 2.3\ i$ and $P(b=0) = 0.45 + 1.6\ i$, for Pb.

$$I_1^{coh}(b) = \frac{k}{4\pi} f_{K_L N \to K_S N}(o)\, T(b)\, e^{-\frac{1}{2}(1 - i\alpha_{KN})\sigma_{KN} T(b)} , \quad (30)$$

which is shown as the solid line in fig. 8. The difference between I_1^{coh} and I_2^{coh} is purely due to different parametrizations of the same model. This indicates that the parameters for the two models we use in our angular distribution calculations are not completely consistent. This discrepancy is due to the uncertainties inherent in the present experimental data for nucleon regeneration, and K_o- and $\bar{K}_o$-nucleon scattering amplitudes, especially the real parts of them.

In this section we have shown the formal equivalence and the detailed difference between the two models. This comparison should be useful for future applications. Finally, we note that the coherent production model is not just an approximation to the optical model. These two models are independent in their physical interpretations of the nuclear regeneration phenomenon. Although the particular models that we describe in this work involve very similar approximations and give similar results, other formalisms of particle-nucleus scattering (with consistent approximations in the coherent production model and the optical model) may give different results.

3. Concluding remarks

We have discussed nuclear $K_L \rightarrow K_S$ regeneration process in terms of the coherent production model, as well as the optical model. We have shown that both models reproduce the experimental data very well, the diffraction pattern being sensitive to nuclear gross size and the normalization to the elementary regeneration parameters. Furthermore, we find no necessity for introducing a neutron radius larger than the proton radius.

We have also shown that the two models are formally equivalent. However, the coherent production formalism may provide us a simpler framework to study separately the nucleon regeneration amplitudes and the nuclear effects. The optical model, on the other hand, provides directly a relation to the K_o and $\bar{K}_o$ elastic scattering amplitudes, which allows us to interrelate these amplitudes and study their detailed behavior. The interrelation of various elastic and regeneration scattering amplitudes is especially useful since we may also calculate the regeneration amplitude directly from the coherent production model.

Quite importantly, we find that the nuclear regeneration process provides a framework of unique interest in the study of various nuclear multiple-scattering formalisms. In most other types of high-energy projectiles, the (uninteresting) diffractive phenomenon prevails so that the main differential cross sections are not sensitive to the model used. We have now a non-diffractive process (the regeneration) which should serve as a much better test of the scattering theory. It may also be argued that large momentum transfer processes with other projectiles should serve the same purpose. However, at large momentum transfers, other more complicated contributions generally occur and these are difficult to take into account.

In conclusion, we would like to suggest some experiments which will help make the regeneration process a useful tool to study nuclear physics. First, in connection with the value of neutron regeneration power and the neutron skin, we would need better data on hydrogen regeneration and nuclear forward regeneration cross sections for various nuclei (preferably with very different neutron excess). Since the neutron enhancement factor γ could be much larger than 1, we would expect the regeneration process to be sensitive to the neutron distribution, and thus provide a chance to determine the neutron radius. In this work, we have shown that the basic character of the differential cross section is related to an overall nuclear matter distribution. This may not remain true in detail when more refined data are available, particularly beyond the first minimum. It would also be useful to extend the experiments to lower energies and lighter nuclei, where various nuclear multiple-scattering theories are most likely to give different results.

Acknowledgments

We would like to thank Eugene Makchowski for his computer programs which we used for part of the calculation, and also Dr. Robert L. Kelly for his careful reading of the manuscript.

References

1) A. Pais and O. Piccioni, Phys. Rev. 100 (1955) 1487

2) M. Gell-Mann and A. Pais, Phys. Rev. 91 (1955) 1387

3) J. D. Jackson, The Physics of Elementary Particles (Princeton University Press, Princeton, New Jersey, 1958) p. 75

4) R. H. Good, R. P. Matsen, F. Muller, O. Piccioni, W. M. Powell, H. S. White, W. B. Fowler, and R. W. Birge, Phys. Rev. 124 (1961) 1223

5) A. Böhm, P. Darriulat, C. Grosso, V. Kaftanov, K. Kleinknecht, H. L. Lynch, C. Rubbia, H. Ticho, and K. Tittel, Phys. Letters 27B (1968) 594; H. Faissner, H. Foeth, A. Staude, K. Tittel, P. Darriulat, K. Kleinknecht, C. Rubbia, J. Sandweiss, M. I. Ferrero, and C. Grosso, Phys. Letters 30B (1969) 204

6) H. Foeth, M. Holder, E. Radermacher, A. Staude, P. Darriulat, J. Deutsch, K. Kleinknecht, C. Rubbia, K. Tittel, M. I. Ferrero and C. Grosso, Phys. Letters 31B (1970) 544

7) K. S. Kölbig and B. Margolis, Nucl. Phys. B6 (1968) 85; Acta. Phys. Polo. B2 (1971) 57

8) Fumiyo Uchiyama, Lawrence Berkeley Laboratory Report, LBL-2045

9) P. G. O. Freund, Phys. Rev. Letters 20 (1968) 235; H. Harari, Phys. Rev. Letters 20 (1968) 1395; H. S. Goldberg and V. L. Telegdi, Phys. Letters 35B (1971) 327

10) W. D. Myers, Phys. Letters 30B (1969) 451

11) See, for example, L. R. B. Elton, Nuclear Sizes, Oxford University Press (1961)

12) A. D. Brody, W. B. Johnson, B. Kehoe, D. W. G. S. Leith, J. S. Loos, G. J. Luste, K. Moriyasu, B. S. Shen, W. M. Smart, F. C. Winkelmann, and R. J. Yamartino, Phys. Rev. Letters 26 (1971) 1050;

P. Darriulat, C. Grosso, M. Holder, J. Pilcher, E. Radermacher, C. Rubbia, M. Scire, A. Staude, and K. Tittel, Phys. Letters 33B (1970) 433

13) W. B. Johnson, D. W. G. S. Leith, J. S. Loos, G. J. Luste, K. Moriyasu, W. M. Smart, F. C. Winkelmann, and R. J. Yamartino, Phys. Rev. Letters 26 (1971) 1053.

14) R. W. Williams, Phys. Rev. 98 (1955) 1387

15) W. L. Wang and R. G. Lipes, Lawrence Berkeley Laboratory Report, LBL-1988 (submitted to Phys. Rev. C)

Table 1. Parameters for K-N Interaction Used in the Calculation at 4.0 GeV/c[a].

Coherent Production Model[b]		Optical Model[b]	
σ_{Kp}	19.65 mb	σ_{K_op}	17.7 mb
σ_{Kn}	21.68 mb	σ_{K_on}	17.2 mb
α_{KN}	- 0.112	α_p	- 0.175
σ_{KN}	20.76 mb	α_n	- 0.328
$(d\sigma_H/dt)_{t=0}$	0.54 mb/(GeV/c)^2	$\sigma_{\bar{K}_op}$	21.01 mb
$(d\sigma_H/dt)_{t=0}$	Experimental data at nearby energies:	$\sigma_{\bar{K}_on}$	25.66 mb
Brody[c] et al.[12]	(0.55 ± 0.18) mb/(GeV/c)^2	$\bar{\alpha}_n$	- 0.003
Darriulat[c] et al.[12]	(0.63 ± 0.38) mb/(GeV/c)^2	$\bar{\alpha}_p$	0.0

[a] The nuclear parameters are $c = 1.2 \times A^{1/3}$ fm and a = 0.6 fm for Woods-Saxon density, eq. (5).

[b] The parameters in these two models are related as:

$$\sigma_{KN} = (Z/A)\ \sigma_{Kp} + (1 - Z/A)\ \sigma_{Kn}$$

$$\sigma_{Kp} = \frac{1}{2}\left(\sigma_{K_op} + \sigma_{\bar{K}_op}\right)$$

$$\sigma_{Kn} = \frac{1}{2}\left(\sigma_{K_on} + \sigma_{\bar{K}_on}\right)$$

$$\alpha_{KN} = \left\{\frac{Z}{A}\left[\alpha_p\ \sigma_{K_op} + \bar{\alpha}_p\ \sigma_{\bar{K}_op}\right] + \left(1 - \frac{Z}{A}\right)\left[\alpha_n\ \sigma_{K_on} + \bar{\alpha}_n\ \sigma_{\bar{K}_on}\right]\right\} \Big/ (2\sigma_{KN}) \quad .$$

[c] The values are obtained by averaging the data over incident momentum from 3-5 (GeV/c).

Figure Captions

Fig. 1. Regeneration of K_S by the coherent production process. The K_L particle is scattered by the nucleus through an optical potential and is changed to a K_S by collision with a single nucleon. The produced K_S is also scattered by the nucleus. ρ and ω trajectories may be exchanged between the K_L and the bound nucleon (CP = -1 exchange).

Fig. 2. Differential $K_L \to K_S$ regeneration cross section for (a) Pb and (b) Cu. The K_L incident momentum is 4 GeV/c. The solid lines are the results of the coherent production model, using the parameter $\alpha = -0.112$ as determined from ref. [8]; the dashed lines are the results of the same calculation using $\alpha = -0.224$. These two values of α give identical results except near the diffraction minimum. The dash-dot lines are the results of the optical model calculations, using the same density distribution for neutrons and protons. The parameters of these calculations are given in Table 1. The data are from Foeth et al.[6]).

Fig. 3. Regeneration of K_S in the optical model description. The incident K_L is considered as a mixture of K_o and $\bar{K}_o$, which are scattered independently through the nucleus with scattering amplitudes F and $\bar{F}$, respectively. The regeneration amplitude for K_S is $F_R^{opt} = \frac{i}{2}(F - \bar{F})$.

Fig. 4. The differential regeneration cross section plotted in the scaling coordinates. The copper and lead data are seen to have a simple scaling property. R is the half radius, $R = 1.2 \times A^{1/3}$ fm of the target. The copper data is multiplied by 4.8, in agreement with the estimate of eq. (19). The differential cross sections are more forward-peaked than the elastic K_o and $\bar{K}_o$ differential cross section, which show the usual diffraction pattern due to strong absorption. The data are from Foeth et al.[6]).

Fig. 5. The scattering amplitudes for K_o and $\bar{K}_o$ on Pb, $F(q^2)$ and $\bar{F}(q^2)$, respectively, and their relative phase $\Phi(q^2)$. Both the magnitudes and the relative phase, i.e. $\cos\Phi$, remain nearly constant only in the small momentum transfer range, beyond which the shape of the regeneration cross section deviates from the K_o-nucleus elastic scattering diffraction pattern (see eq. 21).

Fig. 6. The Regge-pole contributions to the regeneration and elastic amplitudes. The regeneration amplitude is proportional to the difference between the K_o- and $\bar{K}_o$-nucleon elastic scattering amplitudes, where Pomeron (P), A_2 (1100) and f(1270) also contribute. The contributions from P, A_2 and f cancel in the regeneration amplitude due to crossing symmetry.

Fig. 7. Equivalence between the coherent production model and the optical model. The diagrams are obtained by summing both sides of fig. 6 over the nucleons in the nucleus. Using the impulse approximation and neglecting nucleon-nucleon correlations, we may identify the left-hand side with the coherent production model in fig. 1, and the right-hand side with the optical model in fig. 3.

Fig. 8. Detailed behavior of the scattering amplitudes of the two models for Pb. The results are: the solid line (1) the direct parametrization of the coherent production model, from eq. (30); the dashed line (2) the coherent production model using linear combinations of the parameters from the optical model, eq. (28); and the dash-dot line (3) the optical model calculation, from eq. (29). The differences between (1) and (2) are due only to different parametrization of the same model.

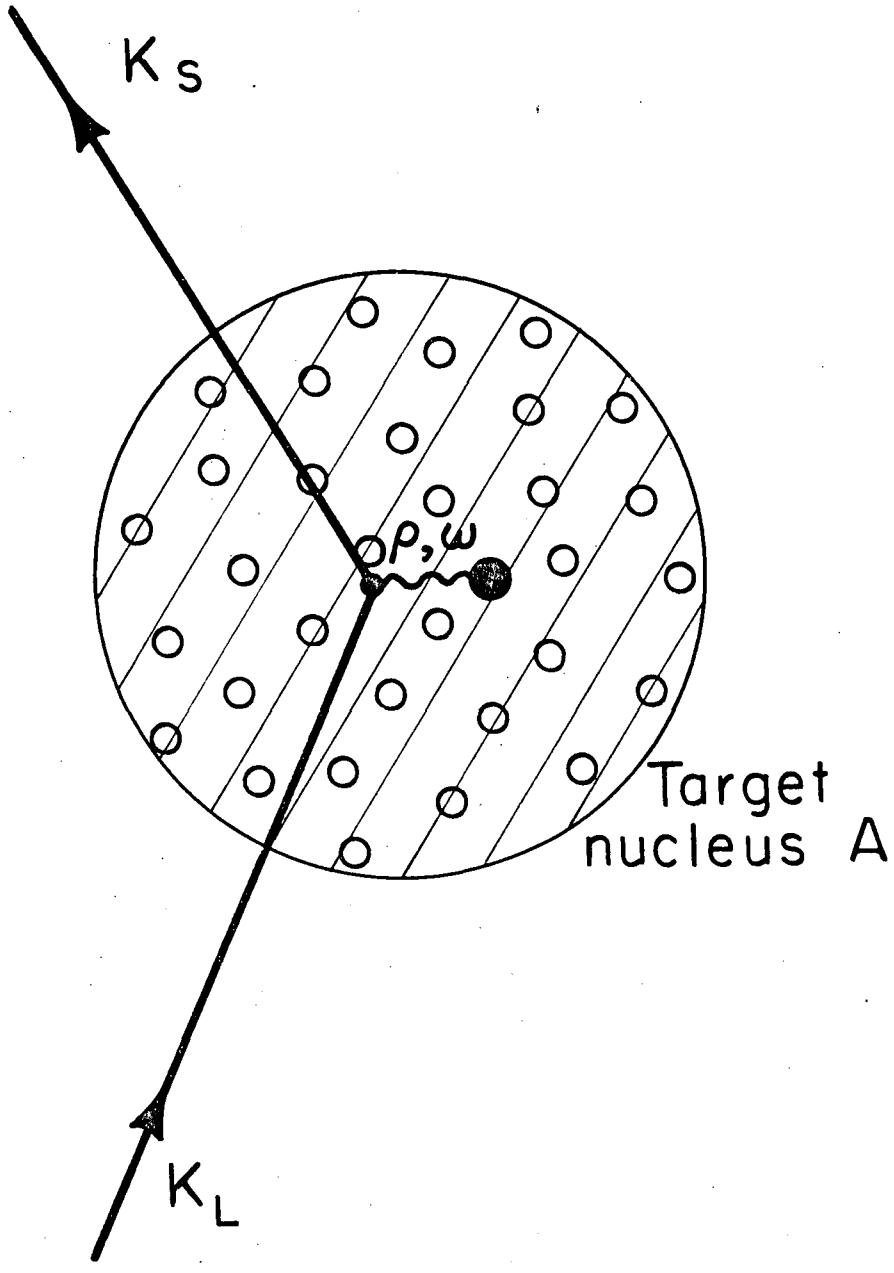

Fig. 1

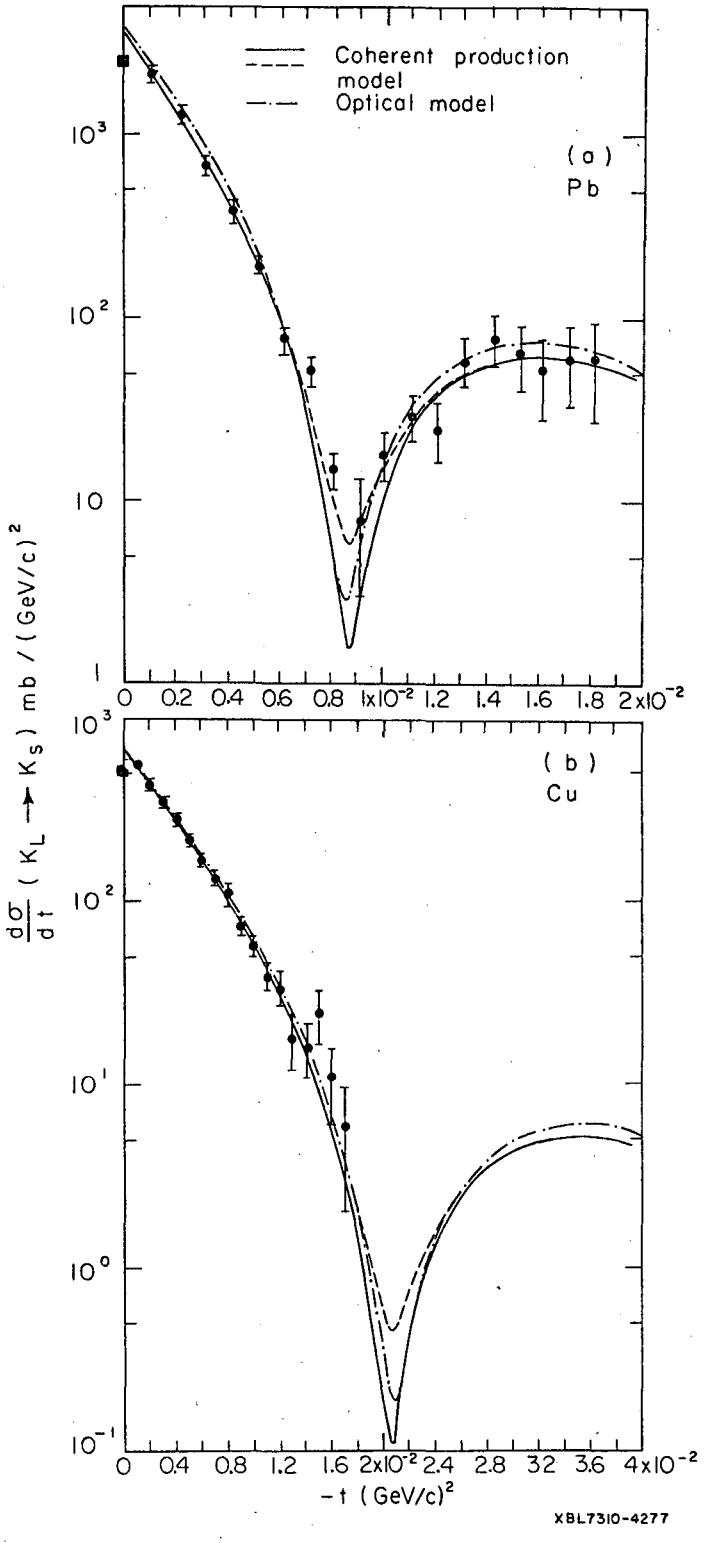
Coherent production model
Optical model
(a)
Pb
(b)
Cu
$\frac{d\sigma}{dt}$ ($K_L \rightarrow K_s$) mb / (GeV/c)^2
10^3
10^2
10
1
10^1
10^0
10^{-1}
0 0.2 0.4 0.6 0.8 1x10^{-2} 1.2 1.4 1.6 1.8 2x10^{-2}
0 0.4 0.8 1.2 1.6 2x10^{-2} 2.4 2.8 3.2 3.6 4x10^{-2}
$-t$ (GeV/c)^2
XBL7310-4277

Fig. 2

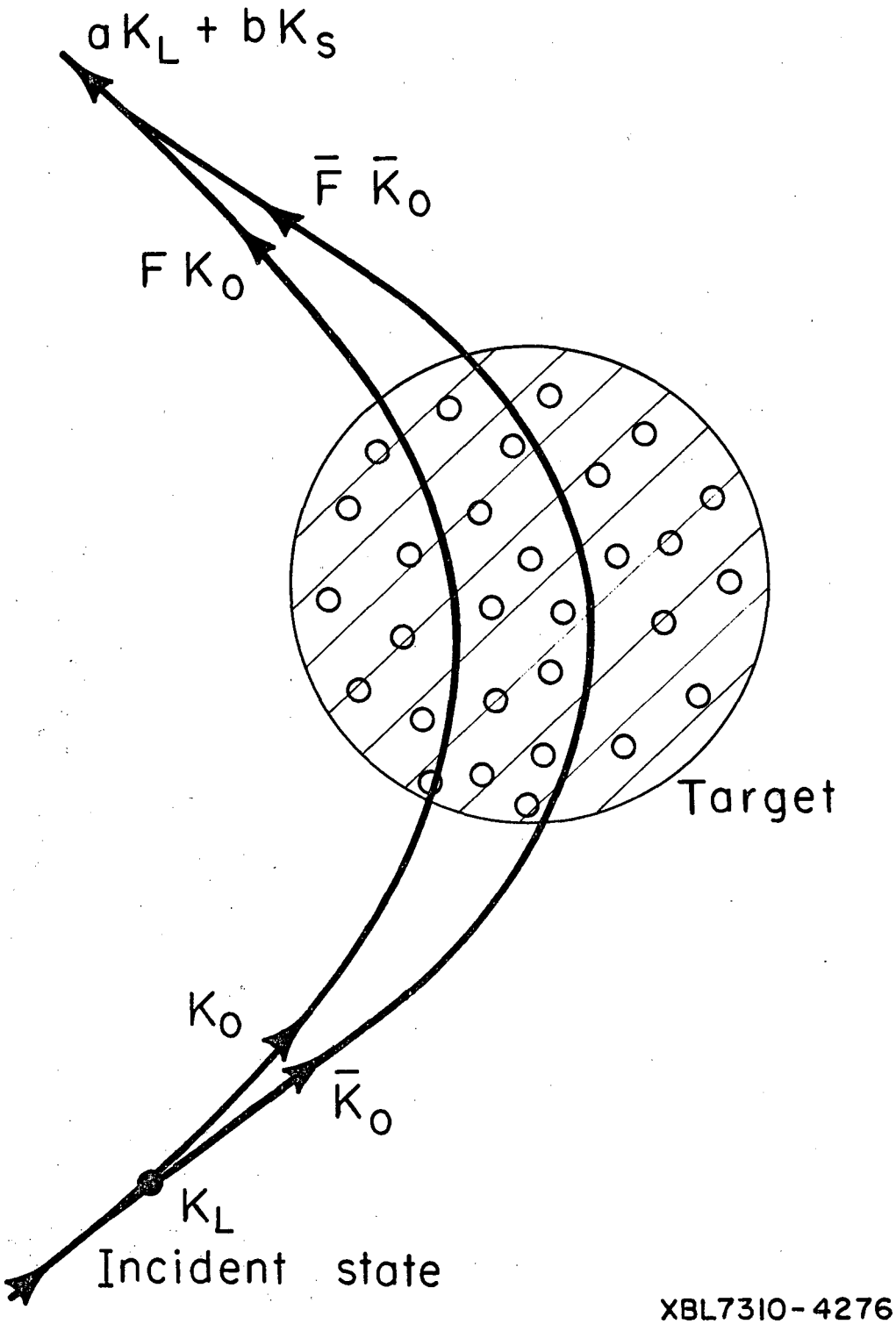
$aK_L + bK_s$
$\bar{F}\,\bar{K}_0$
$F\,K_0$
Target
K_0
$\bar{K}_0$
K_L
Incident state
XBL7310-4276

Fig. 3

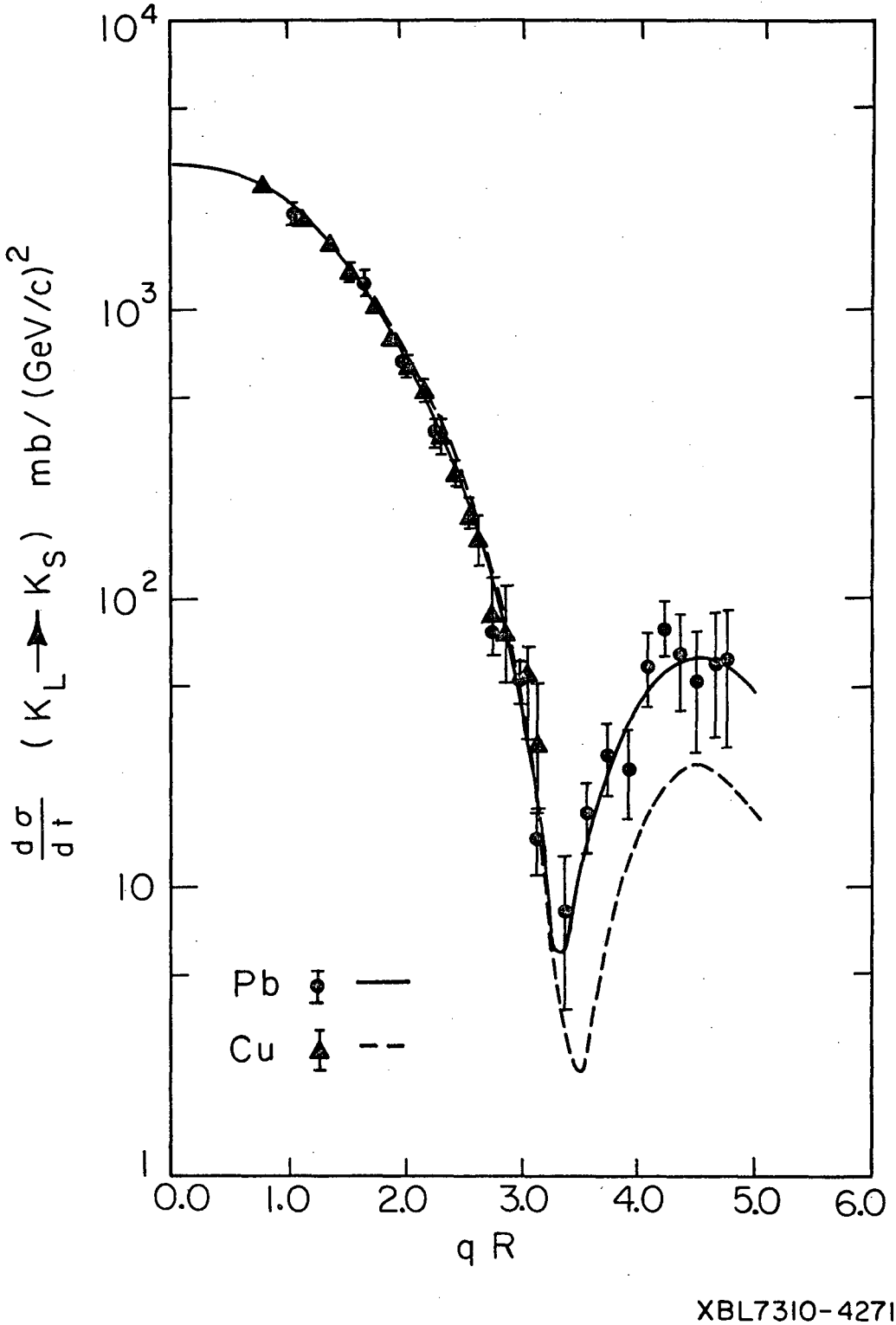
10^4
10^3
10^2
10
1
$\frac{d\sigma}{dt}$ ($K_L \rightarrow K_S$) mb/(GeV/c)^2
Pb
Cu
0.0
1.0
2.0
3.0
4.0
5.0
6.0
q R
XBL7310-4271

Fig. 4

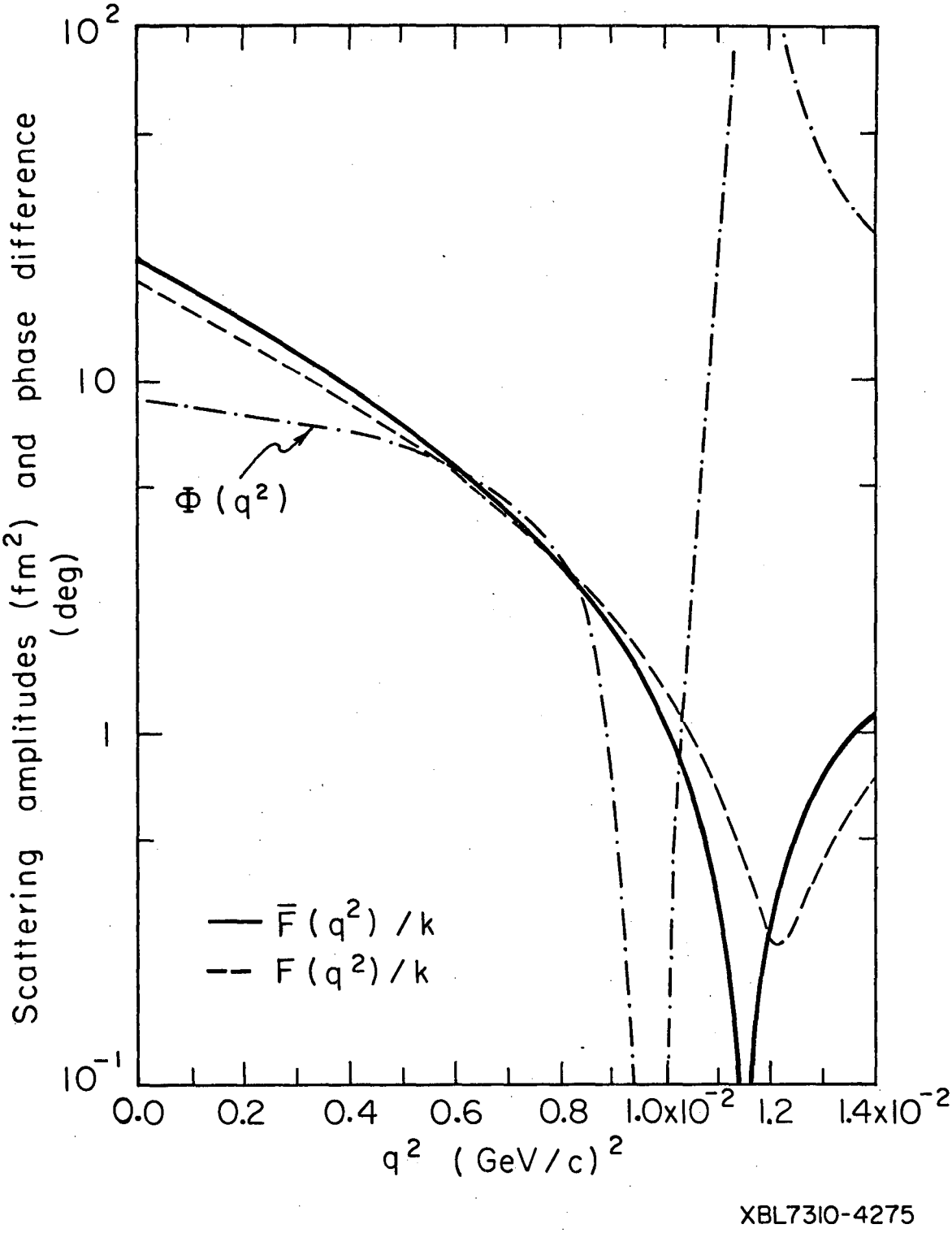
10^2
10
1
10^{-1}
Scattering amplitudes (fm^2) and phase difference (deg)
$\Phi(q^2)$
$\bar{F}(q^2)/k$
$F(q^2)/k$
0.0
0.2
0.4
0.6
0.8
1.0×10^{-2}
1.2
1.4×10^{-2}
q^2 (GeV/c)^2
XBL7310-4275

Fig. 5

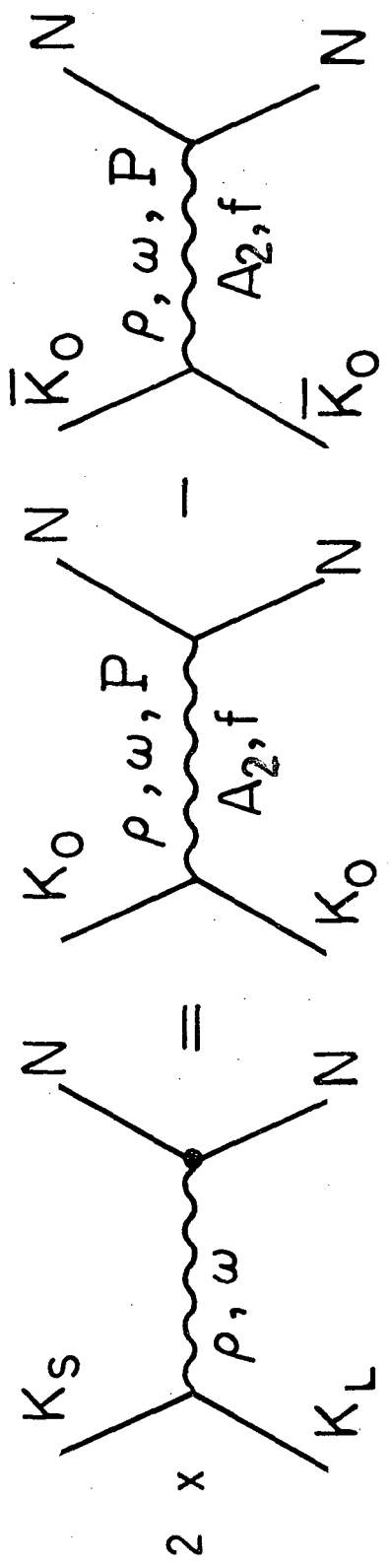

XBL7310-4274

Fig. 6

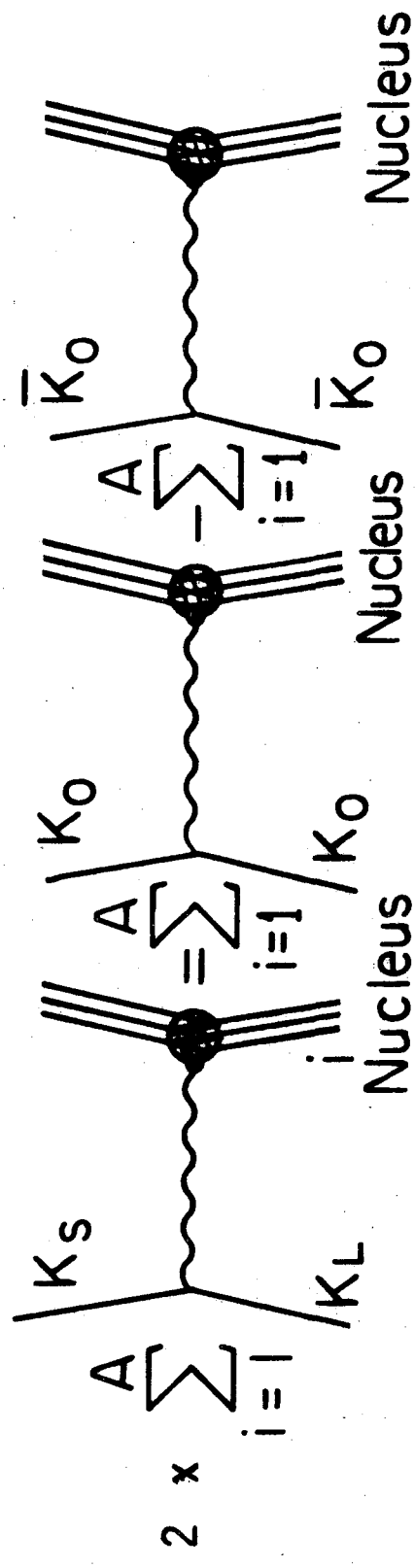

XBL7310-4273

Fig. 7

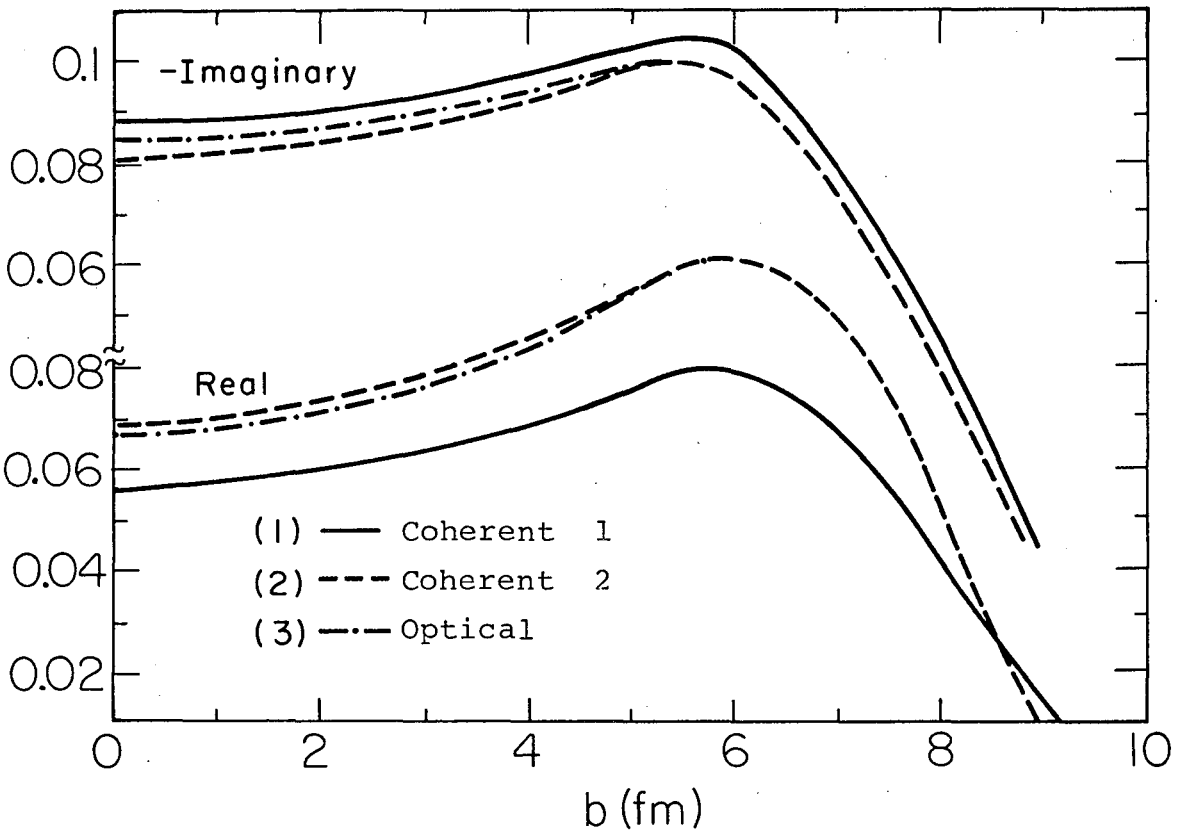
-Imaginary
Real
(1) Coherent 1
(2) Coherent 2
(3) Optical
0.1
0.08
0.06
0.08
0.06
0.04
0.02
0
2
4
6
8
10
b (fm)
XBL7310-4383

Fig. 8

TECHNICAL INFORMATION DIVISION
LAWRENCE BERKELEY LABORATORY
UNIVERSITY OF CALIFORNIA
BERKELEY, CALIFORNIA 94720